# $Nd^{3+}$ doped $LaF_3$ nanoparticles as self-monitored photo-thermal agents

Uéslen Rocha,[1] K. Upendra Kumar,[1] Carlos Jacinto,[1] Julio Ramiro,[2] Antonio J. Caamaño,[2] José García Solé,[3] and Daniel Jaque[3]
[1]*Grupo de Fotônica e Fluidos Complexos, Instituto de Física, Universidade Federal de Alagoas, 57072-970 Maceió, Alagoas, Brazil*
[2]*Department of Signal Theory and Communication, Universidad Rey Juan Carlos, Madrid 28943, Spain*
[3]*Fluorescence Imaging Group, Departamento de Física de Materiales C-04, Facultad de Ciencias, Instituto Nicolás Cabrera, Universidad Autónoma de Madrid, 28049 Madrid, Spain*

(Received 5 November 2013; accepted 9 January 2014; published online 6 February 2014)

In this work, we demonstrate how $LaF_3$ nanoparticles activated with large concentrations (up to 25%) of $Nd^{3+}$ ions can simultaneously operate as biologically compatible efficient nanoheaters and fluorescent nanothermometers under single beam (808 nm) infrared laser excitation. $Nd^{3+}$:$LaF_3$ nanoparticles emerge as unique multifunctional agents that could constitute the first step towards the future development of advanced platforms capable of simultaneous deep tissue fluorescence bio-imaging and controlled photo-thermal therapies. © *2014 AIP Publishing LLC*.
[http://dx.doi.org/10.1063/1.4862968]

Hyperthermia is defined as the procedure of raising the temperature of a part of or the whole body above the normal temperature for a defined period of time.[1] It is being applied, alone or in combination with other therapeutic procedures, as an alternative treatment for several diseases, including cancer. When tumor cells undergone a hyperthermia treatment, the net effects caused on them are strongly dependent on both the magnitude of heating and treatment duration.[2–4] If cell temperature is raised up to temperatures close to 45 °C protein denaturalization and heat-induced cell degradation are simultaneously activated, leading to irreversible damage.[5,6] Temperature induced modification of nuclear proteins have not only the effect of driving cell to death but it is also thought to be the central event by which heat makes tumor cells more "sensitive" to external stimulus leading, for example, to a beneficial synergy between heat and radiation.[7,8] Moreover, the combination of drugs and local heating has also attracted a great attention during last years.[9,10]

The particular method applied to achieve controlled hyperthermia depends on the nature, size, and location of the area to be treated. When treating tumors deeply located into the body, radiofrequency, and microwave radiations should be used in combination with micro antennas.[11,12] On the other hand, for superficial tumors local hyperthermia is achieved by using low frequency waves (microwave or ultrasound waves) generated from a source outside the body. Independently on the particular method used, the heating procedure should be accompanied by real-time thermal reading so that the heating parameters can be properly adjusted thus, controlling the final temperature of the area to be treated.

The fast development of nanotechnology has led to the recent appearance of interesting alternatives for hyperthermia therapies. These are based on the use of bio-compatible nanoparticles (NPs) capable of heating when externally excited.[13] These NPs can be classified into two groups depending on the excitation mechanism: (i) Magnetic NPs (M-NPs), which generate heat when placed in an oscillating external magnetic field and (ii) Photo-thermal NPs (PhT-NPs), in which heat generation is activated under optical excitation.[14–23] PhT-NPs have the advantage that, they can be applied for deep-tissue hyperthermia treatments by using excitation wavelengths lying within the so-called biological windows (spectral ranges where human tissues become partially transparent). When working in these spectral windows, photo-thermal treatments can be highly selective, i.e., light induced hyperthermia is only produced where PhT-NPs have been incorporated. Up to now, several PhT-NPs have been proposed including metallic nanoparticles, semiconductor nanocrystals, graphene nanocrystals, and carbon nanotubes.[19–28] Few previous works have also reported that certain rare earth doped nano-crystals (RE-NPs) could be also used as PhT-NPs, although this possibility has not been demonstrated yet in bio-compatible colloidal solutions.[29] Certain RE-NPs have demonstrated to be highly efficient luminescence probes under excitation with Near Infrared (NIR) radiation within the biological windows.[30–32] An additional advantage of RE-NPs is that they can be used for high resolution fluorescence bioimaging by using CW laser sources; much simpler and affordable that the short pulse lasers required for traditional fluorescence probes used in multiphoton fluorescence microscopy.[33] In addition, the RE-NPs display, in some cases, the additional ability of chemical and thermal luminescence sensing.[32,34] This last feature is of special relevance, since it could be used for thermal monitoring and, hence, for real time controlled photo-thermal therapies. Therefore, the demonstration of efficient light-to-heat conversion in bio-compatible solutions of multi-functional RE-NPs would open avenues for simultaneous fluorescence imaging and treatment of biosystems.

Among many other RE-NPs proposed in the past for fluorescence bio-imaging, $Nd^{3+}$ ion activated $LaF_3$ NPs (hereafter, $Nd^{3+}$:$LaF_3$-NPs) are of special relevance because their unique combination of properties such as high fluorescence quantum yields (well above 50% for medium-low $Nd^{3+}$ ion contents),[32] the possibility of NIR under NIR excitation (NIR-NIR processes), excellent chemical and physical stabilities, and negligible bio-toxicity.[35] In addition to all these properties, $Nd^{3+}$:$LaF_3$ NPs also show fluorescence bands with a remarkable thermal sensitivity.[32] Based on all these

 © 2014 AIP Publishing LLC

properties, $Nd^{3+}$:$LaF_3$-NPs have been recently used for single cell imaging, sub-tissue thermal sensing, and for *in vivo* fluorescence imaging.[35] Light-to-heat conversion in $Nd^{3+}$:$LaF_3$-NPs, not explored yet, would emerge as an important additional feature that would place $Nd^{3+}$:$LaF_3$-NPs in a privilege position among other NPs as they could be used in a multifunctional manner for simultaneous bio-imaging, photo--thermal treatment, and temperature control of the irradiated area, all these facilities with the very same biocompatible nanoprobes.

In this Letter, we demonstrate that this multifunctional operation is possible, as we demonstrate efficient light-to-heat conversion in bio-compatible aqueous solutions of $Nd^{3+}$:$LaF_3$ NPs. The potential application of $Nd^{3+}$:$LaF_3$-NPs for real *in vivo* photo-thermal hyperthermia treatments has been here explored by performing *ex vivo* experiments. Finally, real time temperature monitoring during photo-thermal processes has been demonstrated by taking advantage of the thermal sensitivity of the fluorescence bands of $Nd^{3+}$ ions. We, thus, provide experimental evidence of the potential use of $Nd^{3+}$:$LaF_3$-NPs as a dual system with heating and thermometric properties.

The $Nd^{3+}$:$LaF_3$-NPs used in this work were synthetized at the Universidade Federal de Alagoas by the wet-chemistry method using Lanthanum (III) chloride, Neodymium (III) chloride, and ammonium fluoride reagents as it has been described elsewhere.[36,37] The $Nd^{3+}$ concentration was adjusted by varying the relative content of Neodymium chloride. Up to 5 different $Nd^{3+}$:$LaF_3$-NPs were synthetized with nominal $Nd^{3+}$ concentrations of 2, 5, 15, 20, and 25 at. %. Larger $Nd^{3+}$ concentrations were found to drastically decrease the quality of the obtained nano-particles so that they would not be useful for fluorescence imaging and, consequently, were not investigated in this work. Inset in Figure 1(a) shows a characteristic Transmission Electron Microscopy (TEM) image of the $Nd^{3+}$:$LaF_3$-NPs (25 wt. % $Nd^{3+}$ content). From this image, the size histogram has been calculated and it has been also included in Figure 1(a). The mean NP size has been determined to be 12 nm with a size dispersion of ±5 nm. Both average and size dispersion were found to be independent on the particular $Nd^{3+}$ content. For thermal loading experiments five aqueous dispersions of the $Nd^{3+}$:$LaF_3$-NPs were prepared, all of them with the same nanoparticle concentrations (10% in mass). All the aqueous solutions showed an excellent colloidal behavior without any sign of precipitation for several weeks. Particle agglomeration observed in the TEM image of Figure 1 is very likely occurring during the sample preparation required for the acquisition of TEM images. As an example, Figure 1(c) includes a digital picture of the aqueous solution containing $Nd^{3+}$:$LaF_3$-NPs with a Neodymium concentration of 25 wt. %.

Figure 1(c) schematically shows a simplified energy level diagram of $Nd^{3+}$ ions. The different depopulation processes that are activated when $Nd^{3+}$ ions are optically excited with an 808 nm radiation have been also indicated. After excitation up to the $^4F_{5/2}$ state, nonradiative de-excitation down to the metastable $^4F_{3/2}$ state takes place.[38] Once at the metastable state, $Nd^{3+}$ ions can decay to anyone of the lower energy states ($^4I_{9/2}$, $^4I_{11/2}$, $^4I_{13/2}$, and $^4I_{15/2}$) via a radiative process.[39,40] It should be noted that all the relaxations from the $^4I_J$

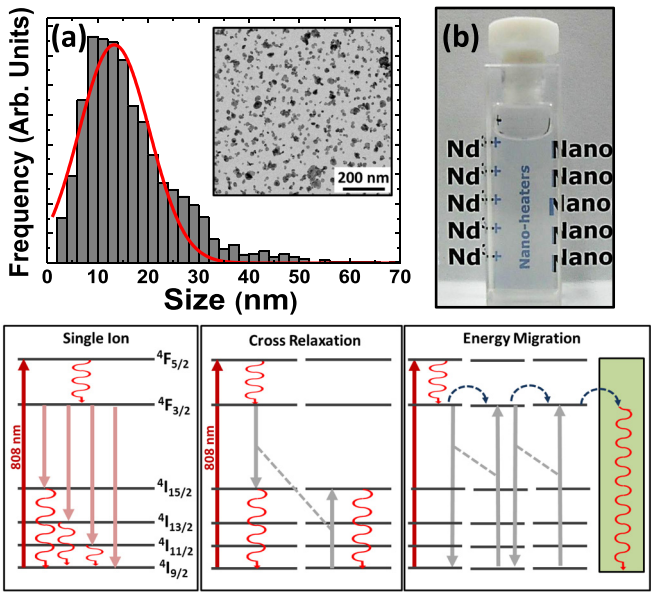


FIG. 1. (a) Size histogram of the $Nd^{3+}$:$LaF_3$ nano-particles as obtained from the analysis of the TEM image, which is included as an inset. Digital picture at the right shows an aqueous solution of $Nd^{3+}$:$LaF_3$ nano-particles. (b)–(d) Schematic diagram of the different radiative and nonradiative processes undergone by Neodymium ions after optical excitation with 808 nm wavelength radiation.

(J = 15/2, 13/2, and 11/2) states to the ground state (J = 9/2) are performed by non-radiative transitions. Since heat is generated with each non-radiative de-excitation, $Nd^{3+}$ ions are expected to partially convert the 808 nm excitation energy into heat. The previous approach applies for $Nd^{3+}$ ions diluted in the host crystal. Indeed, the relaxation dynamic becomes more complicated when the $Nd^{3+}$ content increases. In this case, the distances between neighbor $Nd^{3+}$ ions are reduced and $Nd^{3+}$-$Nd^{3+}$ interactions are activated.[38] This leads to the appearance of both cross relaxation and energy migration processes, which are schematically represented in Figure 1(d). In the first case, de-excitation from the metastable state is achieved by promoting the excitation of a neighboring $Nd^{3+}$ ion from its ground state up to the $^4I_{15/2}$ state. Once both close $Nd^{3+}$ ions are at the $^4I_{15/2}$ state, they de-excite down to the ground state by a multi-phonon relaxation (i.e., delivering heat). In the second case, energy migration between neighboring $Nd^{3+}$ ions occurs until a non-radiative center (*killer*), in which the migrated energy is released, usually by heat generation.[38] According to Figure 1, it is clear that light-to-heat conversion is, indeed, expected in $Nd^{3+}$:$LaF_3$-NPs and that the conversion efficiency should increase with the $Nd^{3+}$ content. Heat generation in 808 nm excited aqueous solutions of $Nd^{3+}$:$LaF_3$-NPs was verified by infrared thermometry. For this purpose, the $Nd^{3+}$:$LaF_3$-NPs/water solutions were placed into open cuvettes. These were excited by a collimated 808 nm laser beam provided by a 100 $\mu$m-core fiber coupled laser diode. The thermal images of the solutions were obtained by imaging the open side of the cuvette with a Fluke Ti10 thermal camera. The thermal images obtained for different $Nd^{3+}$ concentrations (0%, 5%, 15%, and 25%) are shown in Figure 2(a). As can be observed, when the cuvette was filled with pure water, the laser induced thermal loading was negligible. On the other hand, the presence of $Nd^{3+}$:$LaF_3$-NPs in the solution led to a measurable thermal loading whose magnitude increases with the $Nd^{3+}$ ion concentration. This effect

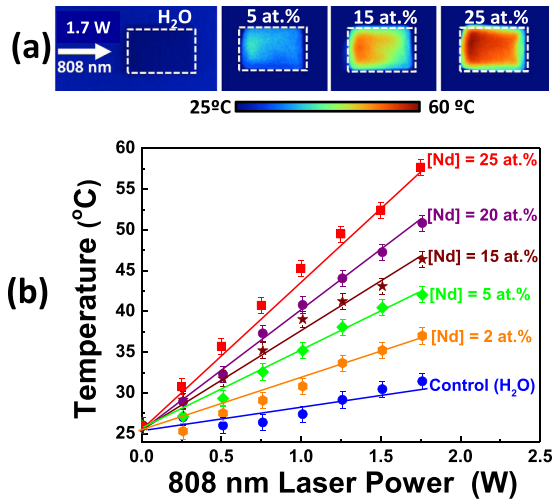


FIG. 2. (a) Steady state infrared thermal images of a cuvette under optical excitation with a 1.7 W 808 laser beam when the cuvette was filled with water and an aqueous solution of $Nd^{3+}$:$LaF_3$ nanoparticles with Neodymium concentrations of 2, 15, and 25 wt. % The nanoparticle concentration in all the solutions was set to 10% in mass. Cuvette dimensions were $1 \times 2$ cm. (b) Steady cuvette temperature as a function of the 808 nm laser power for the different Neodymium contents. Solid symbols are experimental data and lines are the best fits to a linear relation.

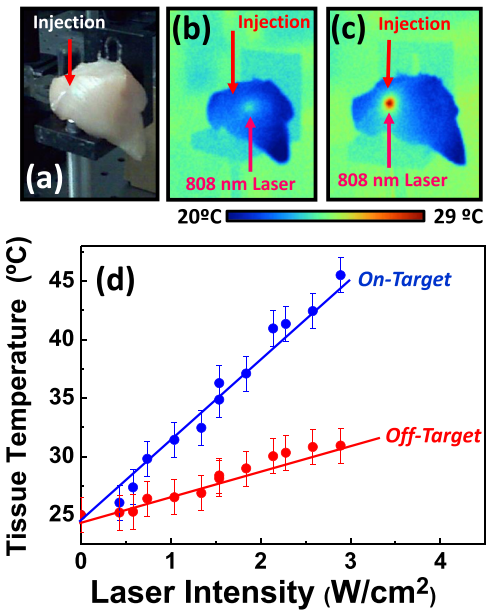


FIG. 3. (a) Optical imaging of the chicken breast used for *ex vivo* photothermal experiments. Arrow indicates the place where the injection of $Nd^{3+}$:$LaF_3$ NPs was performed. (b) and (c) correspond to the thermal images of the chicken breast when illuminated with an 808 nm laser beam (1.5 W/cm$^2$) without and with spatial overlap with the injection of $Nd^{3+}$:$LaF_3$ NPs (*off* and *on-target* situations, respectively). (d) Surface tissue temperature as a function of the 808 nm laser intensity when the beam is illuminating the tissue and the injection (*off* and *on-target*). Dots are experimental data and solid lines are the best fit to a linear relation.

is further evidenced in Figure 2(b), in which we the maximum temperature at the cuvette as a function of the 808 nm laser power is shown for the five available $Nd^{3+}$ concentrations. In all the cases, the temperature increases linearly with the 808 nm laser power. The largest light-to-heat conversion efficiency was found to occur for the largest $Nd^{3+}$ concentration examined in this work (25 at. %). Indeed, this result was expected as larger $Nd^{3+}$ contents result in larger absorption of the incident radiation and, in addition, in lower fluorescence quantum efficiencies (larger light-to-heat conversion efficiencies).[32]

Once the $Nd^{3+}$ ion concentration optimizing the light-to-heat conversion efficiency has been identified, we evaluated the potential application of $Nd^{3+}$:$LaF_3$ NPs for photo-thermal treatments in biological systems by performing *ex vivo* experiments. For this purpose, we injected 0.1 ml of the aqueous solution of $Nd^{3+}$:$LaF_3$-NPs (25 wt. % $Nd^{3+}$ concentration and 10% NPs mass) into a chicken breast. The injection depth was estimated to be around 2 mm. Figure 3(a) shows a digital image of the chicken breast used for *ex vivo* experiments; the place where injection was done is indicated by an arrow. The chicken breast was illuminated with the same fiber-coupled 808 nm laser beam with a spot area at the chicken breast of about 0.7 cm$^2$ and with an angle of incidence of 45°. Figure 3(b) shows the thermal image of the chicken breast when the 808 nm laser was not overlapping with the $Nd^{3+}$:$LaF_3$-NPs injection (*off-target*). As can be observed, the weak tissue absorption at 808 nm (below 0.1 cm$^{-1}$) leads to a slight temperature rise in the illuminated surface area close to 2 °C for a 808 nm excitation intensity of 1.5 W/cm$^2$. The increment in tissue surface's temperature as a function of the 808 nm laser intensity is shown in Figure 3(d), from which we have estimated an intrinsic tissue heating rate close to 2 °C/W · cm$^{-2}$ (here, defined as the increment in tissue temperature divided by the 808 nm laser intensity). When the 808 nm laser spot was overlapping with the $Nd^{3+}$:$LaF_3$-NPs injection (*on-target* configuration), the surface temperature increases due to both intrinsic tissue absorption at laser wavelength and thermal diffusion from the injection that is, indeed, expected to heat significantly. In the *on-target* configuration, surface temperature increased up to 10 °C for a laser intensity of 1.5 W/cm$^2$ (see Figure 3(c)). The NPs-induced heating was found to increase linearly with the 808 nm laser intensity at a heating rate close to 7 °C/W · cm$^2$ (see Figure 3(d)). This is more than three times that found in the *off-target* configuration. This notable difference between the heating rates suggests that $Nd^{3+}$:$LaF_3$-NPs could be used as nanoheaters for selective *in vivo* photo thermal treatments, since relevant heating will be only produced in those areas where $Nd^{3+}$:$LaF_3$-NPs are present. Furthermore, the excellent fluorescence emission characteristic of these NPs will also allow for fluorescence localization of the nano-heaters during *in vivo* application and, also, to follow the tumor evolution during the photothermal treatment by means of fluorescence imaging. At this point it should be noted that the laser intensities used in this work (0–3 W/cm$^2$) did not cause any damage in tissue (chicken breast without NPs injection) after irradiation for min. This is in agreement with the fact that the laser intensities used in this work were comparable to those used in *in vivo* photo-thermal treatments based on both Gold Nanorods and Carbon Nanotubes.[41,42] Furthermore, similar laser intensities were used in previous studies regarding 808 nm laser therapies of skeletal muscles in rats in absence of any tissue damage.[43]

Real controlled photo-thermal therapies of deep tumors (not located at surface) would require real time thermal

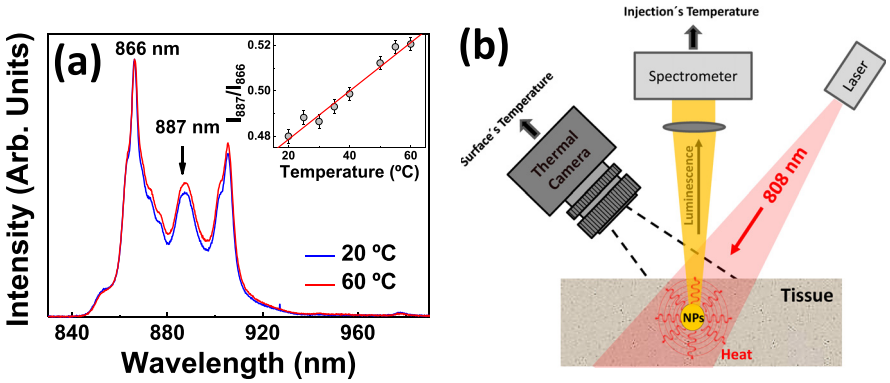


FIG. 4. (a) Emission spectra corresponding to the $^4F_{3/2} \rightarrow {}^4F_{9/2}$ transition generated by an aqueous solution of $Nd^{3+}$:$LaF_3$ NPs as obtained at two different temperatures. Inset shows the temperature dependence of the intensity ratio between the 887 and 866 nm bands. Solids are experimental data and dashed line is the best linear fit. (b) Schematic diagram of the experimental setup used for simultaneous measurement of injection and surface temperatures.

information not in the surface but in the injection volume. In principle, this could be done by taking advantage of the thermal sensitivity of the fluorescence bands of $Nd^{3+}$:$LaF_3$ NPs; i.e., using these NPs as nanothermometers to read out the temperature of the injection. Figure 4(a) shows the $^4F_{3/2} \rightarrow {}^4I_{9/2}$ emission spectrum generated by the aqueous solution containing 25 at. % $Nd^{3+}$ doped $LaF_3$ NPs as obtained at two different temperatures (20 and 60 °C). From a first inspection it is clear that temperature determines the intensity ratio between some emission peaks. Inset in Figure 4(a) shows the ratio between the emission intensities at 887 and 866 nm as a function of temperature, displaying a linear behavior in the range of interest for biological application (20–60 °C). The origin of this temperature induced spectral change has been explained in previous works in terms of the thermal induced re-distributions in the populations of the Stark sub-levels of the $^4F_{3/2}$ metastable state. Briefly, the 887 and 866 nm emission lines are generated by the high and low energy Stark levels of the $^4F_{3/2}$ state, respectively.[32] Thus, from a simple spectral analysis of the luminescence generated by the $Nd^{3+}$:$LaF_3$ injection would provide the actual injection temperature. Since both fluorescence and heat processes are activated by the same 808 nm laser radiation, $Nd^{3+}$:$LaF_3$ NPs could be, in principle, used simultaneously as single/beam excited nano-thermometers and nano-heaters. In order to demonstrate this possibility, we designed the experimental set up depicted in Figure 4(b). This setup allows for simultaneous recording of both surface and injection temperatures by infrared thermometry and spectral analysis of injection fluorescence, respectively. The injection was optically excited in the same configuration as data included in Figure 3. A thermal camera measured the thermal image at an angle of 45°. The fluorescence from the injection was collected by an optical system coupled to a high resolution spectrometer for spectral analysis. Experiments were performed on a 100 $\mu$l injection of an aqueous solution (10% NPs in mass) of $Nd^{3+}$ (25%):$LaF_3$ NPs (injection depth was estimated to be 2 mm). Figure 5(a) shows the emission spectra generated by the $Nd^{3+}$:$LaF_3$ NPs injection as obtained from two different 808 nm laser intensities after 5 min of laser irradiation (time required for complete temperature stabilization). Relevant heating at injection location is evidenced by a clear modification in the emission spectrum. Based on the calibration data included in the inset of Figure 4(a), it was possible to monitor the injection temperature as a function of the 808 nm laser intensity. Results are shown in Figure 5(b). By simultaneously acquiring thermal images of the chicken breast (as that included as an inset in Figure 5(a)), we determined the temperature at tissue surface as a function of laser intensity. Results, again revealing a linear behavior, are also included in Figure 5(b). This figure reveals significant differences between the surface and injection heating rates: 8 and 5 °C/W · cm$^2$, respectively. This means that for a given laser intensity, the injection temperature is almost 60% higher than the temperature at tissue surface. The experimental data included in Figure 5 constitute the demonstration of a self-calibrated photo-thermal process based on a unique

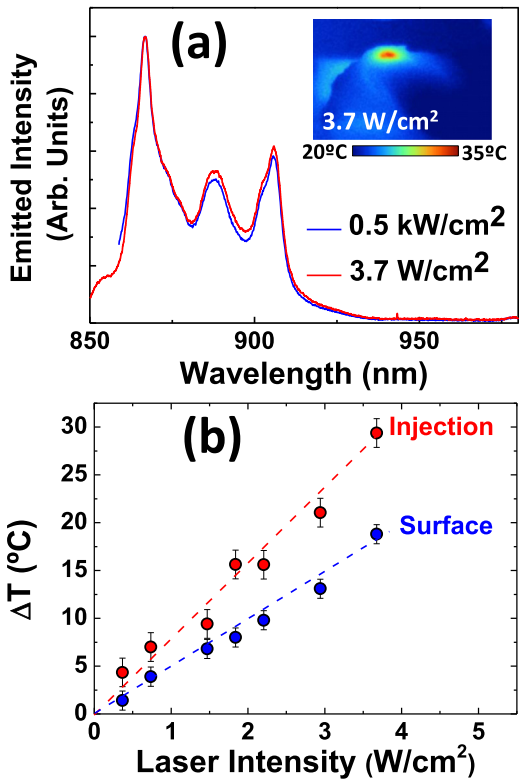


FIG. 5. (a) Emission spectra generated by an injection of $Nd^{3+}$:$LaF_3$ NPs into a chicken breast as obtained for two 808 nm laser intensities. Inset shows the thermal image of the chicken breast when illuminated with a 808 nm laser beam (intensity of 3.7 W/cm$^2$). (b) Laser induced temperature increment at the $Nd^{3+}$:$LaF_3$ NPs injection (determined from the analysis of the sub-tissue emission spectra) as obtained for different 808 nm laser intensities. The temperature increment induced at the surface of chicken breast (determined by infrared thermometry) as a function of the 808 nm laser intensity is also included. Dots are experimental data and dashed lines are the best fits to a linear relation.

nano-particle type and, therefore, opens avenues towards the achievement of single laser beam controlled hyperthermia treatments.

In summary, we have demonstrated that Neodymium doped $LaF_3$ nanoparticles, in addition to be excellent fluorescent bio-labels, can be also used as photo-thermal agents under near-infrared (808 nm) laser illumination. The role played by Neodymium content in the light-to-heat conversion efficiency has been investigated by infrared thermometry. It has been found that higher $Nd^{3+}$ ion contents lead to a larger thermal loading so that a 25% $Nd^{3+}$ concentration per NPs produces substantial heating while still providing enough fluorescent signal for imaging and nanothermometry. *Ex vivo* experiments based on local injection of aqueous solutions of Nd-$LaF_3$ nanoparticles into chicken breast tissues have revealed the potential use of these nano-particles for future selective, high efficient *in vivo* photo-thermal treatments. Furthermore, it has been demonstrated that the thermal sensitivity of the fluorescence bands of $Nd^{3+}$ ions can be used to achieve dynamical sub tissue thermal reading during single beam photo-thermal treatments. All these features confer to $Nd^{3+}$:$LaF_3$ nanoparticles a unique multifunctional character, as they can work as efficient fluorescent nanoprobes, nanoheaters, and nanothermometers under excitation with a sole low power laser source at 808 nm. Thus, the results here reported open an avenue towards the development and design of platforms for the real development of simple and controlled photo-thermal therapies.

This work was supported by the Spanish Ministerio de Educacion y Ciencia (MAT2010-16161 and MAT2010-21270-C04-02), by Brazilian Agencies PRONEX/FAPEAL (Project No. 2009-09-006), by FINEP (Financiadora de Estudos e Projetos), by CNPq (Conselho Nacional de Desenvolvimento Científico e Tecnológico, Grant INCT NANO(BIO)SIMES). Uéslen Rocha is supported by a graduate studentship from CAPES and actually by a PDSE-CAPES program developed in the Universidad Autonoma de Madrid through the Project No. 5990-11-4, Spain. Dr. K.U.K. is supported by a Post Doctoral Fellowship grant of the Programa Nacional de Pós-Doutramento (PNPD/CAPES) at the Universidade Federal de Alagoas (UFAL) through the Project No. 02727/09-9.

[1]R. W. Y. Habash, R. Bansal, D. Krewski, and H. T. Alhafid, CRC Crit. Rev. Bioeng. **34**, 491–542 (2006).
[2]M. Johannsen, U. Gneveckow, L. Eckelt, A. Feussner, N. WaldÖFner, R. Scholz, S. Deger, P. Wust, S. A. Loening, and A. Jordan, Int. J. Hyperthermia **21**, 637–647 (2005).
[3]J. B. Marmor, D. Pounds, T. B. Postic, and G. M. Hahn, Cancer **43**, 188–197 (1979).
[4]J. v. d. Zee and D. G. González, The Lancet **356**, 772 (2000).
[5]B. Hildebrandt, P. Wust, O. Ahlers, A. Dieing, G. Sreenivasa, T. Kerner, R. Felix, and H. Riess, CROH **43**, 33–56 (2002).
[6]W. C. Dewey, Int. J. Hyperthermia **10**, 457–483 (1994).
[7]A. Chicheł, J. Skowronek, M. Kubaszewska, and M. Kanikowski, Rep. Pract. Oncol. Radiother. **12**, 267–275 (2007).
[8]G. M. Hahn, Cancer Res. **34**, 3117–3123 (1974).
[9]Y. Itoh, Y. Kazaoka, M. Nitta, Y. Yamada, and N. Honda, Mol. Med. Rep. **2**, 411–415 (2009).
[10]I. Takahashi, Y. Emi, S. Hasuda, Y. Kakeji, Y. Maehara, and K. Sugimachi, Surgery **131**(1), S78–S84 (2002).
[11]J. C. Lin and Y. J. Wang, Int. J. Hyperthermia **3**, 37–47 (1987).
[12]J. C. Lin and Y. J. Wang, Int. J. Hyperthermia **75**, 1132–1133 (1987).
[13]P. K. Jain, I. H. El-Sayed, and M. A. El-Sayed, Nano Today **2**, 18–29 (2007).
[14]T. Kobayashi, Biotechnol. J. **6**, 1342–1347 (2011).
[15]R. Hergt, S. Dutz, R. Müller, and M. Zeisberger, J. Phys.: Condens. Matter **18**, S2919–S2934 (2006).
[16]P. Tartaj, M. d. P. Morales, S. Veintemillas-Verdaguer, T. Gonzalez-Carreño, and C. J. Serna, J. Phys. D: Appl. Phys. **36**, R182–R197 (2003).
[17]K. S. Martirosyan, J. Nanomed. Nanotechnol. **3**, e-112 (2012).
[18]Q. A. Pankhurst, J. Connolly, S. K. Jones, and J. Dobson, J. Phys. D Appl. Phys. **36**, R167–R181 (2003).
[19]J.-L. Li and M. Gu, IEEE J. Sel. Top. Quantum Electron. **16**, 989–996 (2010).
[20]X. H. Huang, S. Neretina, and M. A. El-Sayed, Adv. Mater. **21**, 4880–4910 (2009).
[21]J. Chen, D. Wang, J. Xi, L. Au, A. Siekkinen, A. Warsen, Z.-Y. Li, H. Zhang, Y. Xia, and X. Xia, Nano Lett. **7**, 1318–1322 (2007).
[22]J. Chen, C. Glaus, R. Laforest, Q. Zhang, M. Yang, M. Gidding, M. J. Welch, and Y. Xia, Small **6**, 811–817 (2010).
[23]S. Sortino, J. Mater. Chem. **22**, 301–318 (2012).
[24]D. K. Chatterjee, P. Diagaradjane, and S. Krishnan, Ther. Delivery **2**, 1001–1014 (2011).
[25]K. H. Baloch, N. Voskanian, M. Bronsgeest, and J. Cumings, Nat. Nanotechnol. **7**, 316–319 (2012).
[26]H. K. Moon, S. H. Lee, and H. C. Choi, ACS Nano **3**, 3707–3713 (2009).
[27]N. W. S. Kam, M. O'Connell, J. A. Wisdom, and H. J. Dai, Proc. Nat. Acad. Sci. U.S.A. **102**, 11600–11605 (2005).
[28]H.-C. Huang, K. Rege, and J. J. Heys, ACS Nano **4**, 2892–2900 (2010).
[29]A. Bednarkiewicz, D. Wawrzynczyk, M. Nyk, and W. Strek, Appl. Phys. B **103**, 847–852 (2011).
[30]R. Weissleder, Nat. Biotechnol. **19**, 316–317 (2001).
[31]A. M. Smith, M. C. Mancini, and S. Nie, Nat. Nanotechnol. **4**, 710 (2009).
[32]U. Rocha, C. Jacinto da Silva, W. F. Silva, I. Guedes, A. Benayas, L. M. Maestro, M. A. Elias, E. Bovero, F. C. J. M. V. Veggel, J. G. Solé, and D. Jaque, ACS Nano **7**, 1188–1199 (2013).
[33]C.-H. Quek and K. W. Leong, Nanomaterials **2**, 92–112 (2012).
[34]D. Wawrzynczyk, A. Bednarkiewicz, M. Nyk, W. Strek, and M. Samoc, Nanoscale **4**(22), 6959–6961 (2012).
[35]U. Rocha, K. U. Kumar, C. Jacinto, I. Villa, F. Sanz-Rodríguez, M. del Carmen Iglesias de la Cruz, A. Juarranz, E. Carrasco, F. C. J. M. van Veggel, E. Bovero, J. G. Solé, and D. Jaque, "Neodymium-doped $LaF_3$ nanoparticles for fluorescence bioimaging in the second biological window," Small (published online).
[36]M. Y. Xie, L. Yu, H. He, and X. F. Yu, J. Solid State Chem. **182**, 597–601 (2009).
[37]F. Wang, Y. Zhang, X. Fan, and M. Wan, J. Mater. Chem. **16**, 1031 – 1034 (2006).
[38]B. H. A. G. F. Imbusch, *Optical Spectroscopy of Inorganic Solids* (Oxford Science, New York, 1989).
[39]V. Lupei, A. Lupei, S. Georgescu, T. Taira, Y. Sato, and A. Ikesue, Phys. Rev. B **64**, 092102 (2001).
[40]G. A. Kumar, C. W. Chen, J. Ballato, and R. E. Riman, Chem. Mater. **19**, 1523–1528 (2007).
[41]L. M. Maestro, P. Haro, B. del Rosal, J. Ramiro, A. J. Caamaño, F. Sanz-Rodríguez, A. Juarranz, E. Carrasco, J. G. Solé, and D. Jaque, Nanoscale **5**, 7882–7889 (2013).
[42]J. T. Robinson, K. Welsher, S. M. Tabakman, S. P. Sherlock, H. L. Wang, R. Luong, and H. J. Dai, Nano Res. **3**(11), 779–793 (2010).
[43]T. Patrocinio, A. C. Sardim, L. Assis, K. R. Fernandes and N. Rodrigues, Photomed. Laser Surg. **31**(10), 492–498 (2013).